IOP Publishing | Institute of Physics and Engineering in Medicine Physics in Medicine & Biology

Phys. Med. Biol. **62** (2017) 6185–6206 https://doi.org/10.1088/1361-6560/aa75b4

Effects of body habitus on internal radiation dose calculations using the 5-year-old anthropomorphic male models

Tianwu Xie[1], Niels Kuster[2,3] and Habib Zaidi[1,4,5,6,7]

[1] Division of Nuclear Medicine and Molecular Imaging, Geneva University Hospital, 1211 Geneva 4, Switzerland
[2] Foundation for Research on Information Technologies in Society (IT'IS), Zeughausstr. 43, 8004 Zurich, Switzerland
[3] Swiss Federal Institute of Technology Zurich (ETHZ), 8092 Zurich, Switzerland
[4] Geneva Neuroscience Center, Geneva University, 1205 Geneva, Switzerland
[5] Department of Nuclear Medicine and Molecular Imaging, University of Groningen, University Medical Center Groningen, 9700 RB Groningen, Netherlands
[6] Department of Nuclear Medicine, University of Southern Denmark, 500 Odense, Denmark

E-mail: habib.zaidi@hcuge.ch

Received 24 January 2017, revised 1 May 2017
Accepted for publication 30 May 2017
Published 13 July 2017

Abstract

Computational phantoms are commonly used in internal radiation dosimetry to assess the amount and distribution pattern of energy deposited in various parts of the human body from different internal radiation sources. Radiation dose assessments are commonly performed on predetermined reference computational phantoms while the argument for individualized patient-specific radiation dosimetry exists. This study aims to evaluate the influence of body habitus on internal dosimetry and to quantify the uncertainties in dose estimation correlated with the use of fixed reference models. The 5-year-old IT'IS male phantom was modified to match target anthropometric parameters, including body weight, body height and sitting height/stature ratio (SSR), determined from reference databases, thus enabling the creation of 125 5-year-old habitus-dependent male phantoms with 10th, 25th, 50th, 75th and 90th percentile body morphometries. We evaluated the absorbed fractions and the mean absorbed dose to the target region per unit cumulative activity in the source region (*S*-values) of F-18 in 46 source regions for the generated 125 anthropomorphic 5-year-old hybrid male phantoms using the Monte Carlo N-Particle eXtended general purpose Monte Carlo transport

[7] Author to whom any correspondence should be addressed.

code and calculated the absorbed dose and effective dose of five ^{18}F-labelled radiotracers for children of various habitus. For most organs, the *S*-value of F-18 presents stronger statistical correlations with body weight, standing height and sitting height than BMI and SSR. The self-absorbed fraction and self-absorbed *S*-values of F-18 and the absorbed dose and effective dose of ^{18}F-labelled radiotracers present with the strongest statistical correlations with body weight. For ^{18}F-Amino acids, ^{18}F-Brain receptor substances, ^{18}F-FDG, ^{18}F-L-DOPA and ^{18}F-FBPA, the mean absolute effective dose differences between phantoms of different habitus and fixed reference models are 11.4%, 11.3%, 10.8%, 13.3% and 11.4%, respectively. Total body weight, standing height and sitting height have considerable effects on human internal dosimetry. Radiation dose calculations for individual subjects using the most closely matched habitus-dependent computational phantom should be considered as an alternative to improve the accuracy of the estimates.

Keywords: radiation dosimetry, hybrid computational phantoms, Monte Carlo, tracers, body habitus

(Some figures may appear in colour only in the online journal)

1. Introduction

Positron emission tomography (PET) is an extremely useful imaging modality for clinical diagnosis, staging, treatment and monitoring of various diseases as it enables the detection and characterization of disease in its early stage and provides valuable diagnostic information, which is not easily obtained using conventional imaging techniques. However, the exposure of patients to ionizing radiation during hybrid imaging examinations (e.g. PET/CT, PET/MRI) is a cause for concern because of the risks of radiation-induced stochastic effects associated with medical radiation procedures, especially for the peadiatric population. At the same absolute level of radiation dose, children may experience higher cancer risks from ionizing radiation than adults (Robbins 2008) and have a longer post-irradiation life period for the emergence of deleterious stochastic effects compared to adults (Steinert *et al* 2003). The accurate assessment of radiation dose delivered to the paediatric population involving the use of diagnostic hybrid imaging techniques is of paramount importance in clinical practice owing to the increased radiation dose compared to single-modelity imaging (Fahey *et al* 2016). The effective dose for a typical whole-body ^{18}F-FDG PET-CT scan was estimated to be about 14–32 mSv for reference adult male patients with an induced cancer risk between 0.2% and 0.5% (Huang *et al* 2009).

Computational phantoms are commonly integrated within dedicated Monte Carlo programs that simulate radiation transport inside the human body to determine the patterns of radiation-tissue interactions and to calculate the absorbed radiation dose in the human body from a variety of different medical radiation sources (Zaidi 1999). The reliability of Monte Carlo calculations is closely linked to the adopted computational model which reflects the physical characteristics (elemental composition and mass density, etc) and anatomical features (shape, volume and size of the body and internal organs) of the human body. Depending on their construction methodology, computational models can be divided into three main categories (Zaidi and Xu 2007). The so-called stylized phantoms which employ simple equation-based mathematical functions to describe idealized arrangements of body organs constitute the first generation of computational phantoms. The second generation of computational phantoms

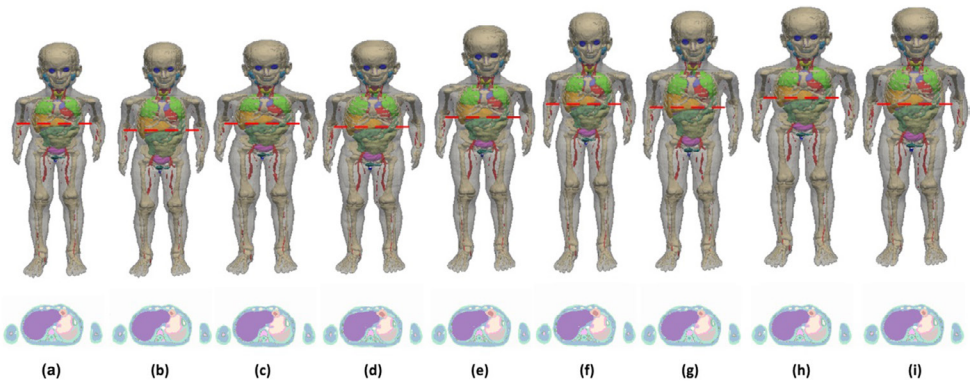

Figure 1. 3D visualization and 2D cross-sections of representative 5-year-old male computational phantoms: (a) 10th weight, 10th height and 10th SSR; (b) 10th weight, 10th height and 90th SSR; (c) 90th weight, 10th height and 10th SSR; (d) 90th weight, 10th height and 90th SSR; (e) 50th weight, 50th height and 50th SSR; (f) 10th weight, 90th height and 10th SSR; (g) 10th weight, 90th height and 90th SSR; (h) 90th weight, 90th height and 10th SSR; (i) 90th weight, 90th height and 90th SSR. The red dot line refers to the level of the illustrated 2D cross-sections.

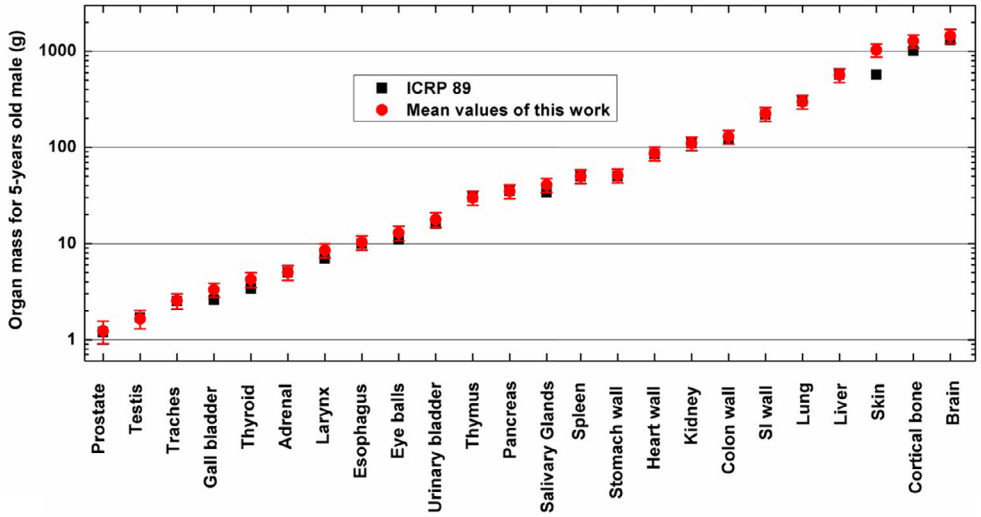

Figure 2. Comparison of organ masses between the generated phantom library of the 5-year-old male and the ICRP reference data. The mean values and 95% confidence intervals are shown.

are voxel phantoms which use digital matrices segmented from computed tomography or magnetic resonance imaging data of humans. The more realistic new-generation of hybrid computational phantoms employ surface-representation methodology by combining the two aforementioned modelling approaches. A total of 38 stylized phantoms, 85 voxel phantoms and 287 hybrid phantoms were reported within in the past 50 years since the development of the first phantom in the 1960s (Xu 2014).

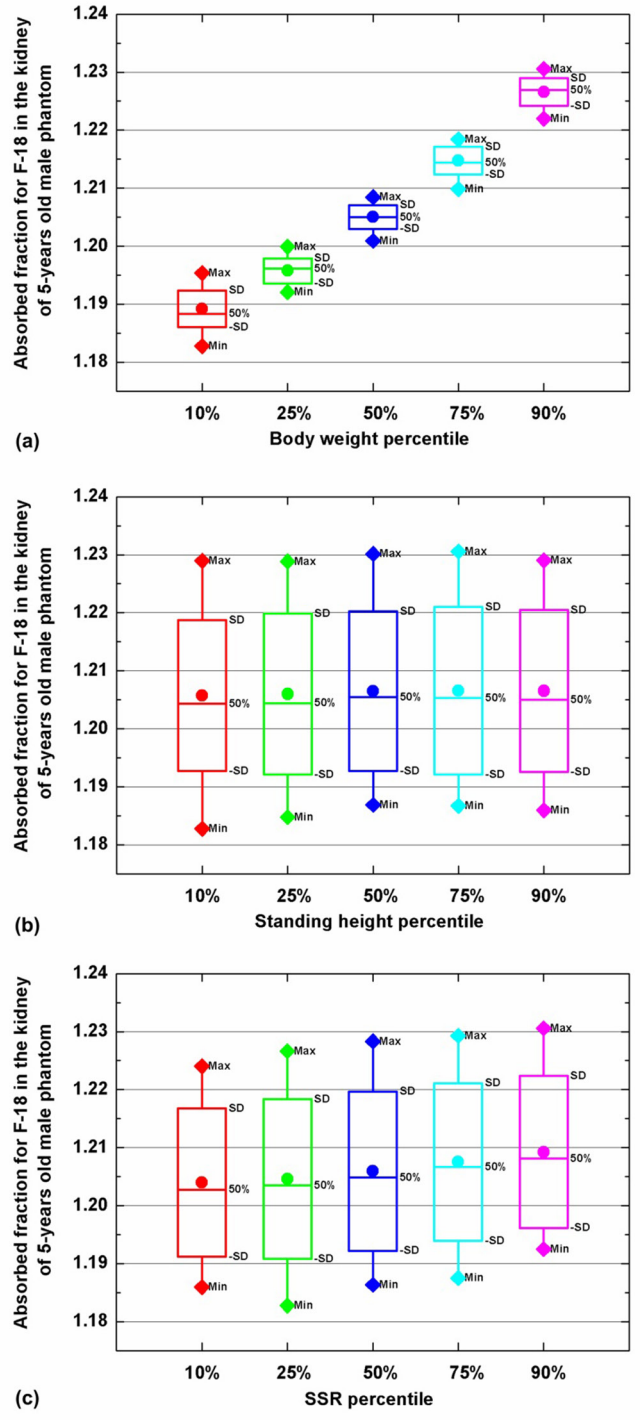

Figure 3. Correlation of self-AFs of F-18 for the kidney with (a) body weight, (b) standing height and (c) SSR for the 5-year-old male phantom series. Statistical parameters (mean, median, min., max. and SD) are also shown.

Table 1. Pearson correlation coefficients for the relationship between body habitus (weight, height, BMI, SSR and Sit. height) and self-AFs of F-18 for representative organs of the 5-year-old male phantoms.

Self-AF of F-18 in organs	Weight	Height	BMI	SSR	Sit. height
Adrenal	0.809[a]	0.140	0.638[a]	0.114	0.180
Brain	0.944[a]	−0.297[a]	0.968[a]	−0.022	−0.253[a]
Kidney	0.983[a]	0.022	0.847[a]	0.178	0.128
Esophagus	0.920[a]	−0.153	0.877[a]	0.053	−0.092
Lymph node	0.825[a]	−0.137	0.790[a]	0.051	−0.078
Liver	0.954[a]	0.163	0.753[a]	0.244[a]	0.281[a]
Lung	0.958[a]	0.157	0.760[a]	0.229	0.268[a]
Pancreas	0.880[a]	0.273[a]	0.635[a]	0.266[a]	0.383[a]
Spleen	0.947[a]	0.147	0.756[a]	0.211	0.250[a]
Thymus	0.949[a]	0.059	0.798[a]	0.169	0.152
Thyroid	0.813[a]	−0.286[a]	0.850[a]	0.074	−0.183
Cortical bone	0.965[a]	−0.238[a]	0.960[a]	0.012	−0.185
Spongiosa	0.963[a]	−0.171	0.925[a]	−0.085	−0.192
Colon	0.978[a]	0.054	0.828[a]	0.186	0.158
Gall bladder	0.892[a]	0.191	0.685[a]	0.275[a]	0.322[a]
Heart	0.952[a]	0.164	0.752[a]	0.255[a]	0.289[a]
Small intestine	0.988[a]	−0.015	0.869[a]	0.155	0.084
Stomach	0.923[a]	0.249[a]	0.685[a]	0.276[a]	0.371[a]
Urinary bladder	0.863[a]	0.300[a]	0.608[a]	0.344[a]	0.456[a]
Total body	0.973[a]	−0.225	0.959[a]	0.087	−0.127

[a] $p < 0.01$.

In traditional medical radiation dosimetry and radiation protection, absorbed doses to fixed age-dependent reference phantoms are assigned to individual patients. Stabin and Siegel (2003) reported *S*-values of 800 radionuclides for the adult male and female as well as paediatric subjects at different ages using the MIRD stylized phantoms. Xie *et al* (2013) and Xie and Zaidi (2014) evaluated the internal dose from positron-emitting radionuclides and radiotracers in the peadiatric population using the University of Florida-National Cancer Institute (UF-NCI) phantom series (Lee *et al* 2005, 2006, 2007). In most studies reported in the literature, the estimation of absorbed dose to patients from radiotracers are performed using pre-calculated dosimetric data for predefined computational phantoms specified in the ICRP reports (ICRP 1987, 1998, 2008), MIRDOSE (Stabin 1996) or OLINDA (Stabin *et al* 2005) packages. With the development of high performance computing, modelling methodology and advanced simulation tools, a paradigm change for the question whether we should continue using a limited number of predefined reference phantoms to represent a population of individuals for internal dosimetry and radiation protection is becoming evident (Zaidi and Xu 2007, Xu and Eckerman 2009, Xu 2014). To answer this question, a comparison of internal radiation doses delivered to computational phantoms of varying body habitus and fixed reference phantoms is highly desired.

New generation hybrid computational phantoms provide a more realistic representation of the anatomical structures of the human body and are more suitable for deformation. For instance, Lee *et al* developed the UF-NCI hybrid phantom series where the total body and internal organs of the produced hybrid phantoms were adjusted to match the reference values of the ICRP publication 89 (Lee *et al* 2005, 2006, 2007). More recently, the Virtual Population

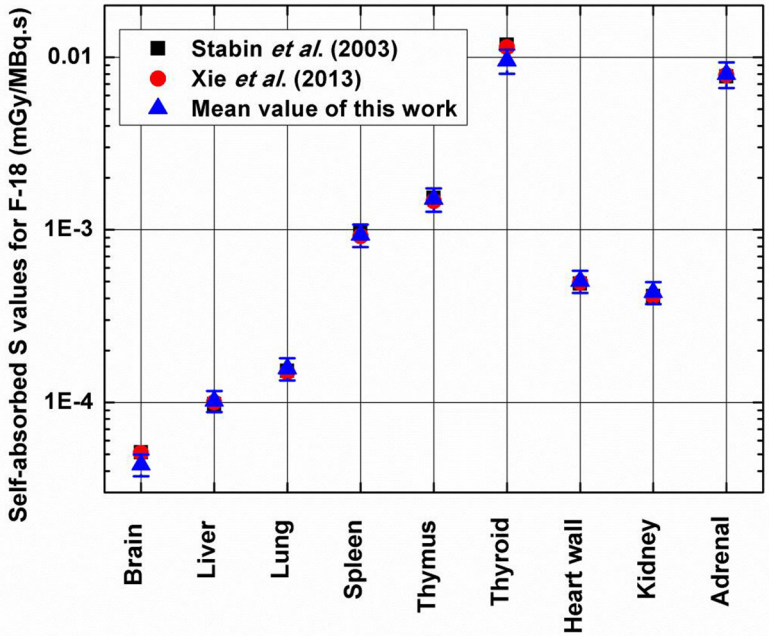

Figure 4. Comparisons of self-absorbed *S*-values for selected internal organs between the results of Stabin and Siegel (2003), Xie *et al* (2013) and this work. The mean values and 95% confidence intervals of the results of this work are shown.

(ViP) phantom library was developed at the IT'IS Foundation for non-ionizing radiation dosimetry applications (Christ *et al* 2010, Gosselin *et al* 2014). This library represents a series of surface-based anatomical models created by segmenting more than 300 tissues and organs from whole body MR images of volunteers, ranging from the newborn, paediatric, adult to elderly subjects, including an obese and pregnant woman. Physics-based morphing techniques were employed to change the posture and change BMI or individual organ weight, enabling a broader range of applications and safety scenarios (Lloyd *et al* 2016).

By adopting a remodelling methodology, a hybrid computational phantom library of the peadiatric population of different body morphometries was recently developed by our group (Xie *et al* 2017). The choice of parameters to investigate was motivated by the fact that the body height, weight and BMI were reported to have statistical correlations with some organs in autopsy studies (de la Grandmaison *et al* 2001, Sheikhazadi *et al* 2010, Molina and DiMaio 2015). In this work, we assess the influence of body habitus on internal radiation dose using the developed 5-year-old anthropometric male phantom library of different body weight, body height and sitting height/stature ratio (SSR). A total of 125 habitus-dependent computational phantoms with 10th, 25th, 50th, 75th and 90th body morphometries were used in Monte Carlo simulations-based calculations of the absorbed fractions (AFs) and *S*-values of F-18 in 46 source regions. Thereafter, the absorbed dose and effective dose of five ^{18}F-labelled radiotracers were evaluated. Dose comparisons were then performed between habitus-dependent phantoms of different anthropometric measurements and the predefined phantoms according to the ICRP reference data.

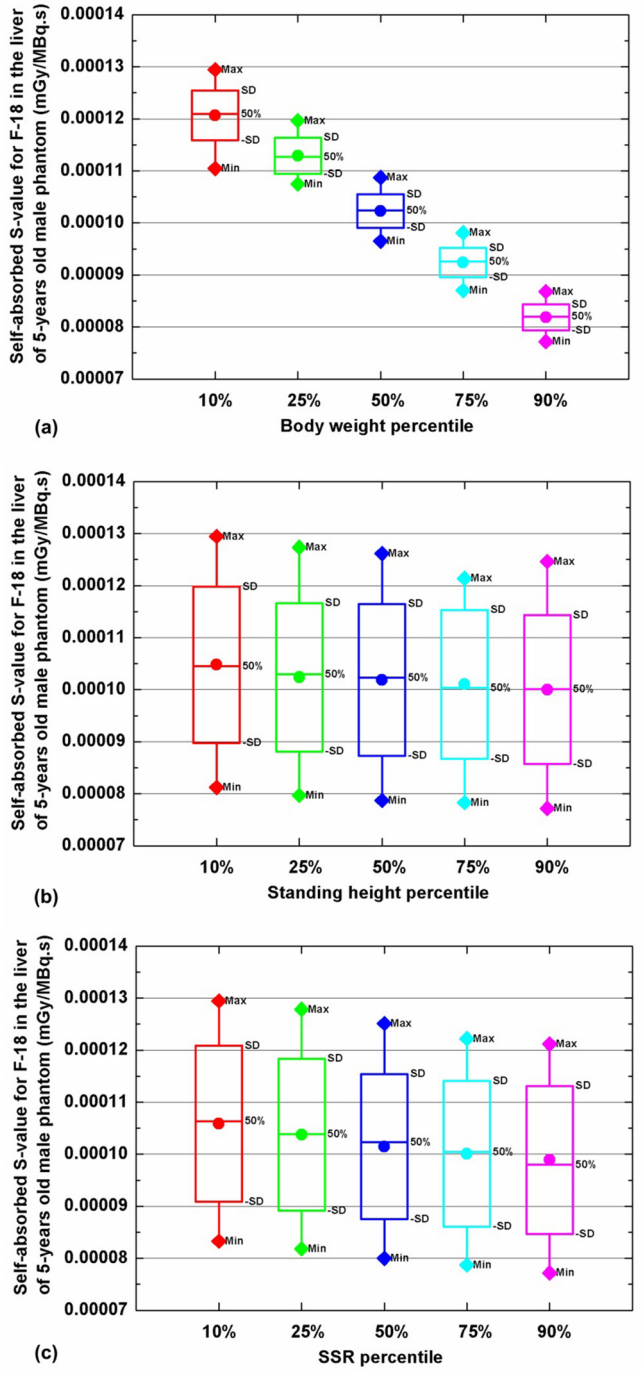

Figure 5. Correlation of self-absorbed *S*-values of F-18 for the liver with (a) body weight, (b) standing height and (c) SSR for the 5-year-old male phantom series. Statistical parameters (mean, median, min., max. and SD) are also shown.

Table 2. Pearson correlation coefficients for the relationship between body habitus (weight, height, BMI, SSR and Sit. height) and self-absorbed *S*-values of F-18 for representative organs of the 5-year-old male phantoms.

Self-absorbed *S*-values of F-18 in organs	Weight	Height	BMI	SSR	Sit. height
Adrenal	−0.889[a]	−0.142	−0.710[a]	−0.126	−0.190
Brain	−0.941[a]	0.295[a]	−0.962[a]	0.026	0.254[a]
Kidney	−0.962[a]	−0.121	−0.785[a]	−0.230	−0.240[a]
Esophagus	−0.945[a]	−0.037	−0.808[a]	−0.192	−0.148
Lymph node	−0.846[a]	−0.090	−0.697[a]	−0.167	−0.175
Liver	−0.966[a]	−0.108	−0.794[a]	−0.219	−0.223
Lung	−0.963[a]	−0.131	−0.781[a]	−0.224	−0.243[a]
Pancreas	−0.956[a]	−0.093	−0.792[a]	−0.205	−0.201
Spleen	−0.941[a]	−0.148	−0.755[a]	−0.225	−0.260[a]
Thymus	−0.939[a]	−0.134	−0.759[a]	−0.212	−0.238[a]
Thyroid	−0.867[a]	0.267[a]	−0.885[a]	−0.043	0.188
Cortical bone	−0.991[a]	0.034	−0.883[a]	−0.041	0.003
Spongiosa	−0.987[a]	0.023	−0.874[a]	0.007	0.025
Colon	−0.961[a]	−0.137	−0.777[a]	−0.225	−0.249[a]
Gall bladder	−0.920[a]	−0.108	−0.754[a]	−0.227	−0.226
Heart	−0.964[a]	−0.109	−0.793[a]	−0.233[a]	−0.231[a]
Small intestine	−0.961[a]	−0.140	−0.776[a]	−0.230[a]	−0.255[a]
Stomach	−0.963[a]	−0.116	−0.789[a]	−0.225	−0.233[a]
Urinary bladder	−0.956[a]	−0.100	−0.790[a]	−0.235[a]	−0.227
Total body	−0.992[a]	−0.053	−0.843[a]	−0.055	−0.075

[a] $p < 0.01$.

2. Materials and methods

2.1. Construction of computational phantoms with different body habitus

The targeted anthropometric parameters, including 10th, 25th, 50th, 75th and 90th percentiles of body weight, body height and SSR for the 5-year-old male, were obtained from the National Health and Nutrition Examination Surveys (NHANES) dataset (Frisancho 2008, McDowell *et al* 2008). In these anthropometric parameters, total body weight, body height and BMI represent general indicators for the size of a patient and characterize the percentage of body fat. With the determined body weight and BMI, the standing height, which limits the variability in both sitting height and leg length can be calculated. The sitting height is given by the product of standing height and SSR while the leg length is calculated by subtracting sitting height from standing height. The sitting height and leg length are used as starting points for phantom remodelling. The paediatric models at different age of the IT'IS phantom series (Gosselin *et al* 2014) were used as anchor phantoms for the generation of new hybrid models of the paediatric population at corresponding ages. To generate the 5-year-old male phantoms, the 5-year-old female Roberta model (V3.0) was used as anchor phantom and deformed using the Visualization Toolkit (VTK) (Xie *et al* 2017). Sex-specific organs were replaced by scaling the corresponding organs of the 14 years-old adolescent model (Charlie).

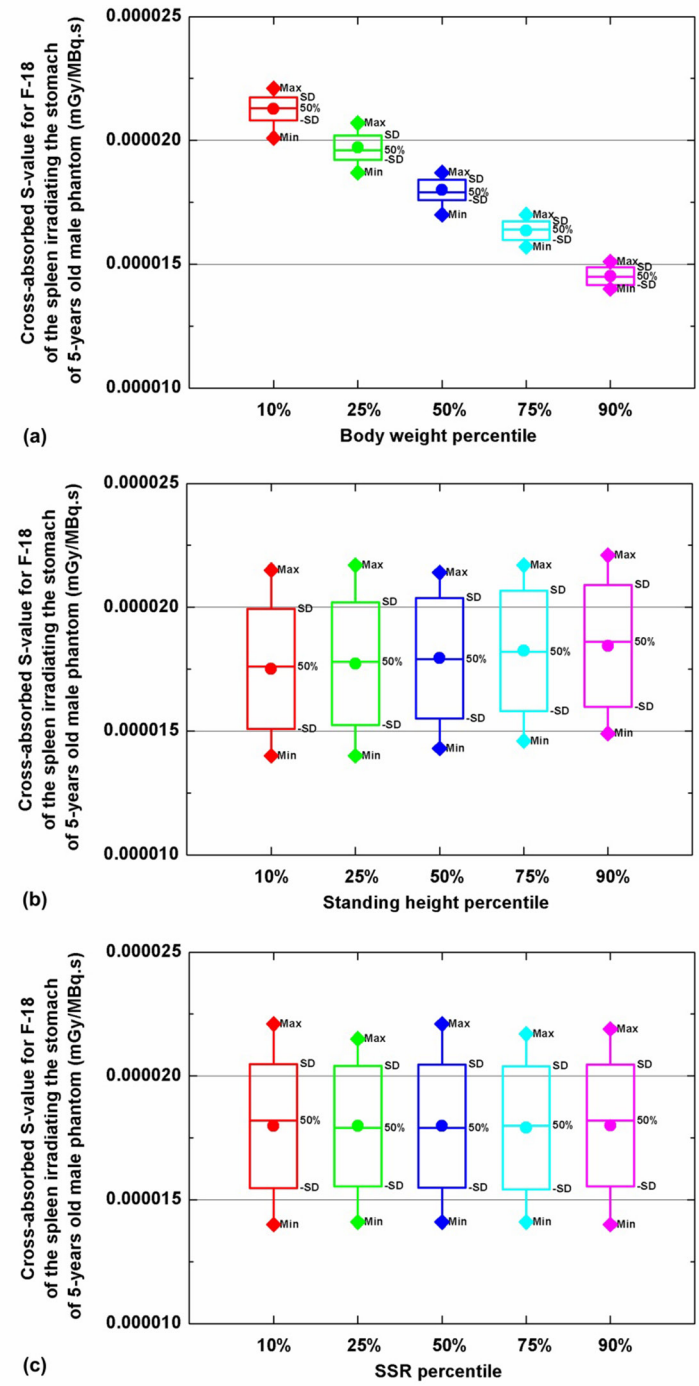

Figure 6. Correlation of cross-absorbed *S*-values of F-18 for the spleen irradiating the stomach with (a) body weight, (b) standing height and (c) SSR for the 5-year-old male phantom series. Statistical parameters (mean, median, min., max. and SD) are also shown.

Table 3. Pearson correlation coefficients for the relationship between body habitus (weight, height, BMI, SSR and Sit. height) and cross-absorbed *S*-values of F-18 for representative organ pairs of the 5-year-old male phantoms.

Cross-absorbed *S*-values of F-18 in various organ pairs						
Sources	Targets	Weight	Height	BMI	SSR	Sit. height
Colon	Urinary bladder	−0.911[a]	−0.247[a]	−0.681[a]	−0.281[a]	−0.372[a]
Colon	Stomach	−0.871[a]	−0.322[a]	−0.612[a]	−0.345[a]	−0.473[a]
Colon	SI	−0.947[a]	−0.180	−0.744[a]	−0.265[a]	−0.309[a]
Colon	Heart	−0.328[a]	−0.758[a]	0.071	−0.492[a]	−0.914[a]
Heart	Urinary bladder	0.067	−0.808[a]	0.448[a]	−0.479[a]	−0.946[a]
Heart	Stomach	−0.793[a]	−0.438[a]	−0.489[a]	−0.399[a]	−0.600[a]
Heart	SI	−0.216	−0.789[a]	0.185	−0.498[a]	−0.943[a]
Kidney	Urinary bladder	−0.146	−0.809[a]	0.256[a]	−0.490[a]	−0.954[a]
Kidney	Stomach	−0.956[a]	−0.115	−0.783[a]	−0.229	−0.234[a]
Kidney	SI	−0.980[a]	0.027	−0.871[a]	−0.159	−0.077
Kidney	Heart	−0.754[a]	−0.461[a]	−0.447[a]	−0.433[a]	−0.640[a]
Kidney	Colon	−0.977[a]	−0.058	−0.827[a]	−0.186	−0.162
Kidney	Total	−0.990[a]	−0.071	−0.833[a]	−0.071	−0.099
Kidney	Spleen	−0.887[a]	−0.310[a]	−0.632[a]	−0.271[a]	−0.416[a]
Kidney	Pancreas	−0.979[a]	0.112	−0.910[a]	−0.082	0.040
Kidney	Lung	−0.342[a]	−0.763[a]	0.062	−0.478[a]	−0.909[a]
Kidney	Liver	−0.928[a]	−0.221	−0.708[a]	−0.292[a]	−0.359[a]
Liver	Urinary bladder	−0.043	−0.834[a]	0.360[a]	−0.464[a]	−0.957[a]
Liver	Stomach	−0.980[a]	0.150	−0.928[a]	−0.078	0.073
Liver	SI	−0.904[a]	−0.273[a]	−0.664[a]	−0.323[a]	−0.420[a]
Liver	Heart	−0.900[a]	−0.281[a]	−0.656[a]	−0.335[a]	−0.435[a]
Liver	Colon	−0.748[a]	−0.494[a]	−0.421[a]	−0.405[a]	−0.648[a]
Liver	Total	−0.991[a]	−0.061	−0.839[a]	−0.071	−0.092
Liver	Spleen	−0.945[a]	0.278[a]	−0.957[a]	0.018	0.235[a]
Liver	Pancreas	−0.981[a]	−0.001	−0.858[a]	−0.157	−0.098
Liver	Lung	−0.658[a]	−0.545[a]	−0.320[a]	−0.474[a]	−0.732[a]
Lung	Urinary bladder	0.045	−0.834[a]	0.440[a]	−0.446[a]	−0.946[a]
Lung	Stomach	−0.683[a]	−0.546[a]	−0.340[a]	−0.437[a]	−0.710[a]
Lung	SI	−0.204	−0.780[a]	0.193	−0.517[a]	−0.948[a]
Lung	Heart	−0.989[a]	0.012	−0.871[a]	−0.144	−0.079
Lung	Colon	−0.276[a]	−0.773[a]	0.126	−0.502[a]	−0.932[a]
Lung	Total	−0.993[a]	−0.027	−0.856[a]	−0.059	−0.056
Lung	Spleen	−0.625[a]	−0.609[a]	−0.259[a]	−0.437[a]	−0.760[a]
Lung	Pancreas	−0.487[a]	−0.715[a]	−0.090	−0.452[a]	−0.855[a]
Pancreas	Urinary bladder	0.059	−0.844[a]	0.458[a]	−0.405[a]	−0.927[a]
Pancreas	Stomach	−0.975[a]	−0.086	−0.814[a]	−0.183	−0.183

(*Continued*)

Table 3. (*Continued*)

Cross-absorbed *S*-values of F-18 in various organ pairs						
Sources	Targets	Weight	Height	BMI	SSR	Sit. height
Pancreas	SI	−0.806[a]	−0.431[a]	−0.503[a]	−0.364[a]	−0.571[a]
Pancreas	Heart	−0.438[a]	−0.713[a]	−0.047	−0.492[a]	−0.878[a]
Pancreas	Colon	−0.915[a]	−0.186	−0.714[a]	−0.327[a]	−0.353[a]
Pancreas	Total	−0.989[a]	−0.073	−0.831[a]	−0.058	−0.092
Pancreas	Spleen	−0.949[a]	0.146	−0.902[a]	0.013	0.126
Small intestine	Urinary bladder	−0.503[a]	−0.674[a]	−0.122	−0.479[a]	−0.839[a]
Small intestine	Stomach	−0.702[a]	−0.545[a]	−0.356[a]	−0.428[a]	−0.704[a]
Spleen	Urinary bladder	−0.155	−0.782[a]	0.233[a]	−0.492[a]	−0.933[a]
Spleen	Stomach	−0.978[a]	0.138	−0.921[a]	−0.064	0.073
Spleen	SI	−0.849[a]	−0.342[a]	−0.585[a]	−0.360[a]	−0.499[a]
Spleen	Heart	−0.984[a]	0.060	−0.891[a]	−0.132	−0.034
Spleen	Colon	−0.857[a]	−0.316[a]	−0.601[a]	−0.343[a]	−0.465[a]
Spleen	Total	−0.991[a]	−0.049	−0.844[a]	−0.064	−0.078
Stomach	Urinary bladder	0.003	−0.819[a]	0.393[a]	−0.479[a]	−0.954[a]
Total	Urinary bladder	−0.991[a]	−0.066	−0.836[a]	−0.076	−0.098
Total	Stomach	−0.992[a]	−0.047	−0.846[a]	−0.066	−0.077
Total	SI	−0.991[a]	−0.068	−0.835[a]	−0.078	−0.101
Total	Heart	−0.992[a]	−0.053	−0.843[a]	−0.065	−0.081
Total	Colon	−0.991[a]	−0.065	−0.837[a]	−0.073	−0.096

[a] $p < 0.01$.

An in house developed C++ program was used to perform the phantom construction according to targeted anthropometric parameters. The deformation process includes three main steps. In the first step, the anchor phantom is divided into torso and leg parts where these two parts are uniformly scaled to match the targeted sitting height and leg length. Once the sitting height and leg length have been adjusted to achieve the target values, the new torso and leg models are merged into a new voxel model with the desired SSR and standing height. In the next step, the new voxel model is automatically reconstructed into a polygon mesh model using VTK, and then subsequently modified to match the targeted body weight and BMI. The aimed body weight is achieved by scaling the mesh model in two dimensions, which involves iterating between estimating the total body mass and adjusting the scaling factors for internal organs and body contour. The organ mass is calculated as the product of the organ volumes and their corresponding densities for the paediatric population of various ages. The total body weight is determined as the sum of masses of all identified organs and residual tissues, where the organ density is obtained from the ICRP 89 report (ICRP 2002). The final step consists in voxelizing the remodelled mesh model into a voxel model. More detailed information about the conceptual design of the library of computational models is given in Xie *et al* (2017).

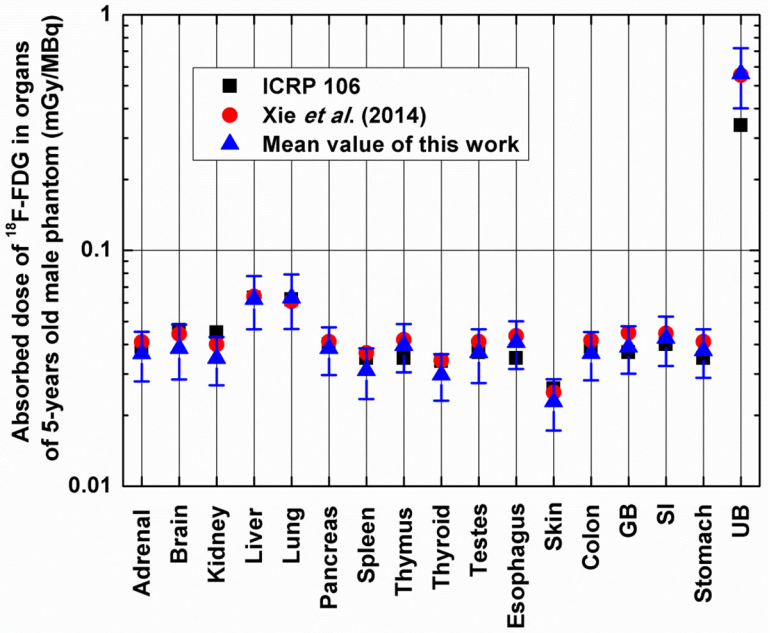

Figure 7. Comparison of the absorbed dose of ^{18}F-FDG between the results of the ICRP 106 (ICRP 2008), Xie and Zaidi (2014) and this work for representative internal organs. The mean values and 95% confidence intervals of the results of this work are shown.

2.2. Monte Carlo simulations

The 125 generated computational phantoms of the 5-year-old male are used as input to the MCNPX Monte Carlo code (Pelowitz 2005) to simulate the transport and interaction of the emitted radiation. A uniform voxel dimension of $2 \times 2 \times 3\,\text{mm}^3$ was set for all voxel phantoms to minimize the differences across different models. The number of voxels of each identified organ/region is calculated and multiplied by the voxel volume and corresponding tissue density to yield the organ/region mass. The chemical composition of each organ is obtained from the ICRP report 89 (ICRP 2002). Uniformly distributed F-18 is simulated in 46 identified organs for the 125 constructed computational models. The decay scheme of F-18 was obtained from the Health Physics Society electronic resource (HPS 2012). AFs and *S*-values of the considered radionuclides are calculated for all source-target pairs of the 125 models. In all simulations, a total of 1.0×10^7 primary particle histories were generated resulting in a statistical uncertainty in terms of coefficient of variation (COV) of less than 2% in most of the cases.

The calculated *S*-values of F-18 were used to estimate the absorbed dose and effective dose of ^{18}F-labelled radiotracers for the 5-year-old male phantoms of different habitus. The investigated radiotracers include ^{18}F-FDG (2-[^{18}F]Fluoro-2-deoxy-D-glucose) to study glucose metabolism (Reivich *et al* 1985), ^{18}F-Amino acids to study protein synthesis (Huang and McConathy 2013), ^{18}F-Brain receptor substances for molecular imaging of cerebral receptors (Huang and McConathy 2013), ^{18}F-L-dopa (6-[^{18}F]Fluoro-L-dopa) to study dopamine metabolism and dopaminergic function (Oehme *et al* 2011) and ^{18}F-FBPA (4-borono-2-^{18}F-fluoro-L-phenylalanine) to predict the effect of boron neutron capture therapy (Yoshimoto *et al* 2013). The biokinetic data of these radiotracers were obtained from the supplemental material of the ICRP reports (ICRP 2008, 1998).

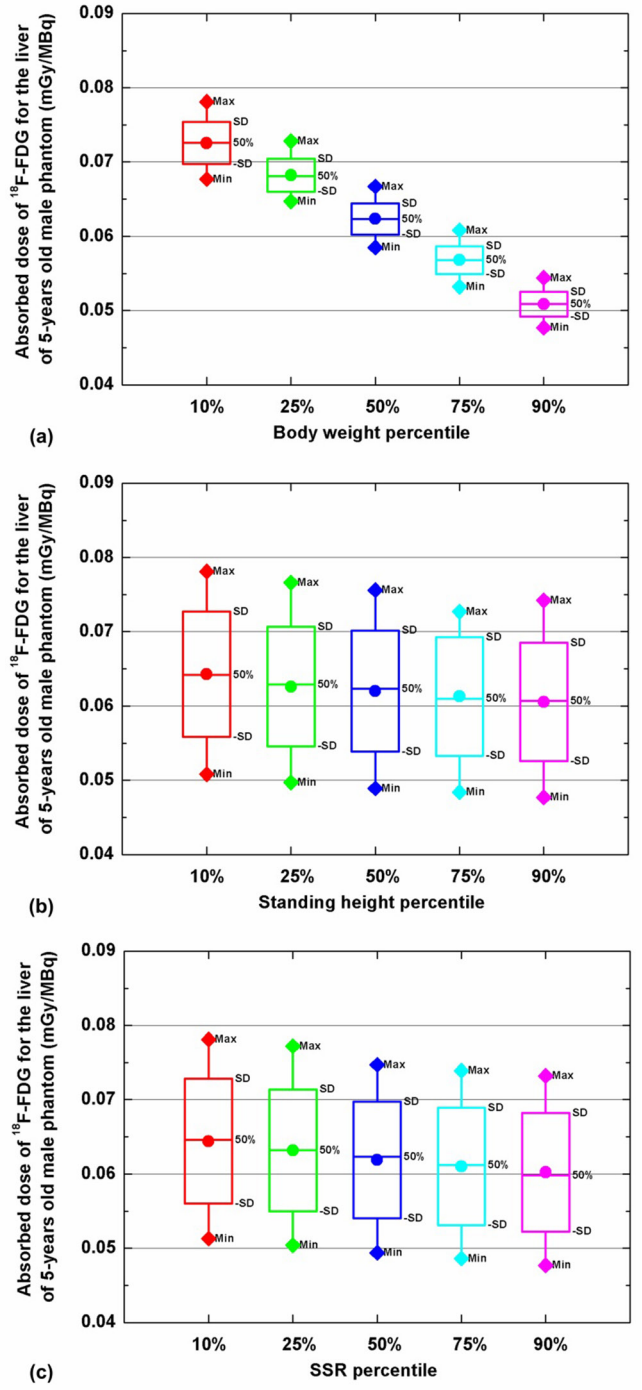

Figure 8. Correlation of the absorbed dose of ^{18}F-FDG in the liver with (a) body weight, (b) standing height and (c) SSR for the 5-year-old male phantom series. Statistical parameters (mean, median, min., max. and SD) are also shown.

Table 4. Pearson correlation coefficients for the relationship between body habitus (weight, height, BMI, SSR and Sit. height) and absorbed dose of ^{18}F-FDG and ^{18}F-FBPA for representative organs of the 5-year-old male phantoms.

Absorbed dose of ^{18}F-FDG in organs	^{18}F-FDG					^{18}F-FBPA				
	Weight	Height	BMI	SSR	Sit. height	Weight	Height	BMI	SSR	**Sit. Height**
Adrenal	−0.942[a]	−0.200	−0.730[a]	−0.180	−0.270[a]	−0.938[a]	−0.206	−0.724[a]	−0.181	−0.276[a]
Brain	−0.957[a]	0.247[a]	−0.952[a]	0.013	0.207	−0.976[a]	0.168	−0.932[a]	−0.007	0.132
Kidney	−0.945[a]	−0.219	−0.724[a]	−0.238[a]	−0.323[a]	−0.956[a]	−0.162	−0.760[a]	−0.234[a]	−0.276[a]
Liver	−0.959[a]	−0.156	−0.765[a]	−0.226	−0.265[a]	−0.955[a]	−0.176	−0.752[a]	−0.229	−0.283[a]
Lung	−0.964[a]	−0.149	−0.773[a]	−0.214	−0.252[a]	−0.961[a]	−0.170	−0.761[a]	−0.212	−0.267[a]
Pancreas	−0.935[a]	−0.232[a]	−0.709[a]	−0.250[a]	−0.341[a]	−0.939[a]	−0.219	−0.718[a]	−0.244[a]	−0.326[a]
Salivary glands	−0.978[a]	0.138	−0.920[a]	−0.021	0.099	−0.976[a]	0.145	−0.921[a]	−0.017	0.107
Spleen	−0.955[a]	−0.177	−0.753[a]	−0.208	−0.271[a]	−0.947[a]	−0.186	−0.742[a]	−0.220	−0.286[a]
Thymus	−0.941[a]	−0.214	−0.723[a]	−0.235[a]	−0.316[a]	−0.945[a]	−0.201	−0.732[a]	−0.216	−0.295[a]
Thyroid	−0.951[a]	0.027	−0.845[a]	−0.113	−0.048	−0.897[a]	0.210	−0.884[a]	−0.057	0.134
Cortical bone	−0.992[a]	−0.025	−0.857[a]	−0.040	−0.043	−0.992[a]	−0.017	−0.861[a]	−0.042	−0.038
Spongiosa	−0.989[a]	−0.039	−0.847[a]	0.002	−0.027	−0.988[a]	−0.049	−0.842[a]	0.007	−0.032
Colon	−0.949[a]	−0.216	−0.728[a]	−0.230[a]	−0.316	−0.954[a]	−0.195	−0.744[a]	−0.223	−0.294[a]
Gall bladder	−0.922[a]	−0.245[a]	−0.691[a]	−0.263[a]	−0.359[a]	−0.927[a]	−0.234[a]	−0.701[a]	−0.256[a]	−0.346[a]
Heart	−0.962[a]	−0.129	−0.781[a]	−0.232[a]	−0.247[a]	−0.958[a]	−0.153	−0.766[a]	−0.234[a]	−0.267[a]
Small intestine	−0.928[a]	−0.254[a]	−0.693[a]	−0.268[a]	−0.370[a]	−0.925[a]	−0.263[a]	−0.686[a]	−0.269[a]	−0.378[a]
Stomach	−0.943[a]	−0.217	−0.724[a]	−0.249[a]	−0.329[a]	−0.936[a]	−0.248[a]	−0.702[a]	−0.248[a]	−0.353[a]
Urinary bladder	−0.957[a]	−0.104	−0.788[a]	−0.233[a]	−0.228	−0.956[a]	−0.107	−0.787[a]	−0.234[a]	−0.231[a]
Skeleton	−0.991[a]	−0.035	−0.850[a]	−0.020	−0.039	−0.991[a]	−0.036	−0.850[a]	−0.018	−0.038
Total body	−0.991[a]	−0.058	−0.840[a]	−0.066	−0.086	−0.991[a]	−0.058	−0.840[a]	−0.066	−0.086

[a] $p < 0.01$.

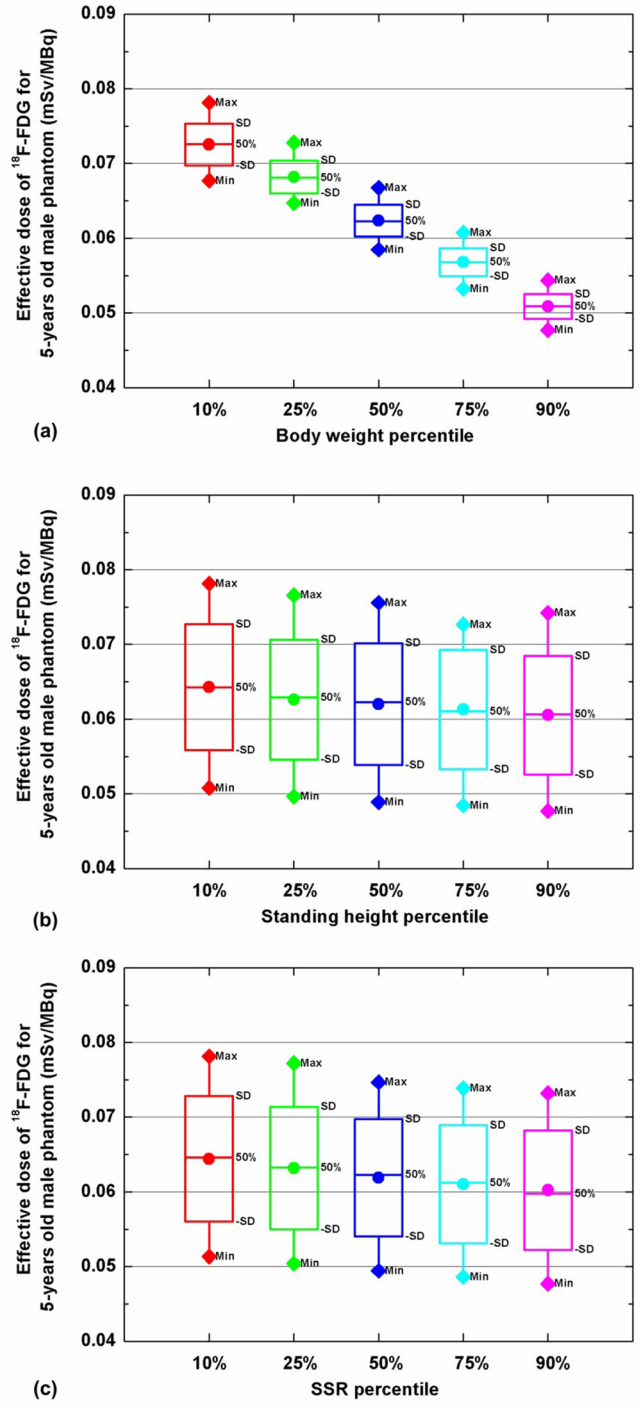

Figure 9. Correlation of effective dose of ^{18}F-FDG for the 5-year-old male phantoms with (a) body weight, (b) standing height and (c) SSR. Statistical parameters (mean, median, min., max. and SD) are also shown.

Table 5. Pearson correlation coefficients for the relationship between body habitus (weight, height, BMI, SSR and Sit. Height) and the effective dose of ^{18}F-Amino acids, ^{18}F-Brain receptor substances, ^{18}F-FDG, ^{18}F-L-DOPA and ^{18}F-FBPA in the 5-year-old male phantoms.

	Weight	Height	BMI	SSR	Sit. Height
^{18}F-Amino acids	−0.934[a]	−0.176	−0.735[a]	−0.108	−0.208
^{18}F-Brain receptor substances	−0.976[a]	−0.107	−0.803[a]	−0.188	−0.202
^{18}F-FDG	−0.968[a]	−0.158	−0.773[a]	−0.189	−0.243[a]
^{18}F-L-DOPA	−0.960[a]	−0.185	−0.752[a]	−0.207	−0.277[a]
^{18}F-FBPA	−0.949[a]	−0.062	−0.801[a]	−0.227	−0.189

[a] $p < 0.01$.

Table 6. Pearson correlation coefficients for the relationship between body habitus parameters (weight, height, BMI, SSR and Sit. height).

	Weight	Height	BMI	SSR
Height	−0.0001			
BMI	0.875[a]	−0.478[a]		
SSR	0.062	−0.036	0.079	
Sit. Height	0.037	0.775[a]	−0.333[a]	0.603[a]

[a] $p < 0.01$.

2.3. Dosimetry calculations

The absorbed dose is the most relevant dosimetric quantity in radiation biology, clinical radiology, and radiological protection. It is defined as the mean energy imparted to the target tissue per unit mass. In the medical internal radiation dose (MIRD) formalism (Bolch *et al* 2009), the radiation absorbed dose $D(r_T, T_D)$ delivered to target tissue r_T from source organ r_S is given by $D(r_T, T_D) = \sum_{r_S} \tilde{A}(r_S, T_D) S(r_T \leftarrow r_S)$ where $S(r_T \leftarrow r_S) = \frac{1}{M(r_T)} \sum_i E_i Y_i \phi(r_T \leftarrow r_S, E_i)$ is the S-value describing the equivalent dose rate in the target organ per unit activity in the source organ. $\tilde{A}(r_S, T_D)$ is the cumulative activity in the source organ over the dose-integration period T_D, E_i is the individual energy of the ith radiation, Y_i is the yield of the ith radiation per nuclear transformation and $M(r_T)$ is the mass of the target organ. $\phi(r_T \leftarrow r_S, E_i)$ is the absorbed fraction given by E_d/E_i, where E_d refers to the deposited energy in the target tissue of the ith radiation emitted from source.

The effective dose is linked to biological risks and relates the absorbed dose to biological effects of radiation by assessing the combined detriments from stochastic effects to all organs. The effective dose is calculated as $E = \sum_T w_T \sum_R w_R D_R(r_T, T_D)$, E is the effective dose, w_T and w_R are the tissue weighting factor for organ T reflecting its relative radiation sensitivity and the radiation weighting factor for radiation type R reflecting the linear energy transfer of radiation, respectively. $D_R(r_T, T_D)$ is the contribution of radiation R to the total absorbed dose (ICRP 2007).

2.4. Parameterization analysis

The effective dose and correlation with body habitus for the corresponding phantom were parameterized using a 2D polynomial function of 10 terms and a least-squares fit for a more

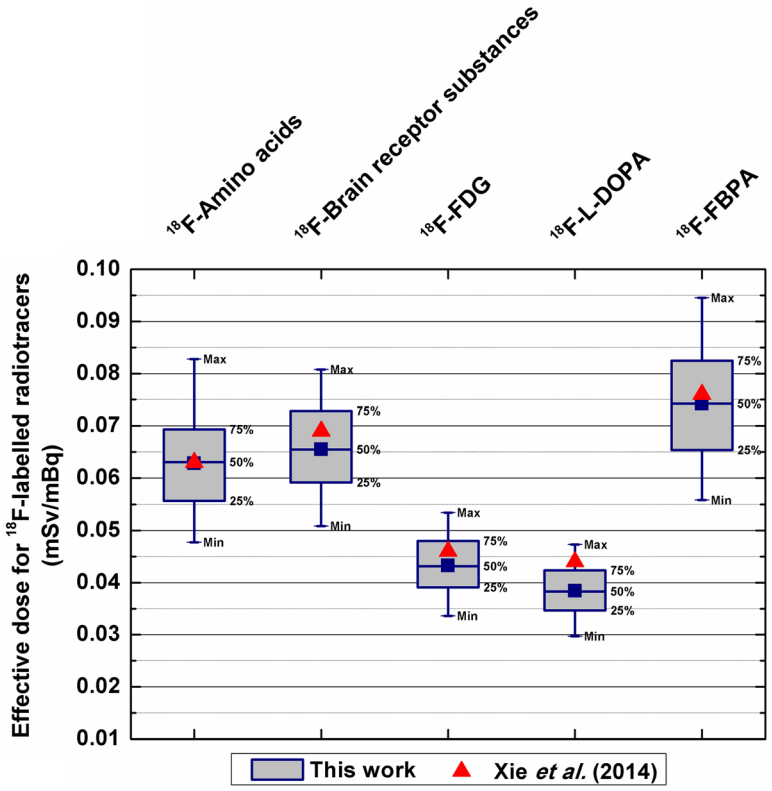

Figure 10. Comparison of the effective dose of ^{18}F-labelled radiotracers for the 5-year-old male between the constructed phantoms and Xie and Zaidi (2014) for the UF-NCI phantom with the ICRP reference data.

convenient presentation of the results The body habitus results were normalized to improve numerical precision (Li *et al* 2013). For the 125 samples of effective dose/body habitus combinations, mean values and standard deviations (SDs) of weight, height and SSR were calculated. They were then used for data normalization while each variable is subtracted by the mean value and divided by the SD. Three normalized measures for the body habitus were adopted:

$$x = \frac{\text{weight} - \overline{\text{weight}}}{\text{SD (weight)}},\ y = \frac{\text{height} - \overline{\text{height}}}{\text{SD (height)}}, z = \frac{\text{SSR} - \overline{\text{SSR}}}{\text{SD (SSR)}}. \quad (1)$$

Each fit of effective dose/body habitus combination resulted in 10 coefficients of a 2D polynomial function.

3. Results

3.1. Organ masses of 5-year-old paediatric phantoms

Figure 1 shows the constructed 5-year-old male phantoms with 10th and 90th weight, 10th and 90th body height, 10th and 90th SSR, and phantom with 50th weight, 50th body height, 50th SSR, respectively. Visual inspection revealed that the constructed peadiatric phantoms

Table 7. Parameterization coefficients of quadratic functions for calculating the effective dose of ^{18}F-Amino acids, ^{18}F-Brain receptor substances, ^{18}F-FDG, ^{18}F-L-DOPA and ^{18}F-FBPA. Three variables (x, y and z) were defined (see equation (1)).

	^{18}F-Amino acids	^{18}F-Brain receptor substances	^{18}F-FDG	^{18}F-L-DOPA	^{18}F-FBPA
1	0.058 107	0.063 224	0.042 553	0.038 965	0.065 680
x	−0.006 234	−0.006 295	−0.004 262	−0.004 020	−0.006 269
y	−0.000 402	−0.000 471	−0.000 839	−0.000 930	−0.001 363
z	−0.000 847	−0.000 500	−0.000 657	−0.000 834	−0.000 964
xy	−0.000 123	0.000 288	0.000 247	0.000 315	0.000 309
xz	0.000 658	0.000 598	0.000 230	0.000 060	0.000 233
yz	-9.30×10^{-05}	-6.97×10^{-05}	5.58×10^{-05}	1.99×10^{-04}	1.17×10^{-04}
x^2	−0.000 467	−0.001 225	−0.000 323	−0.000 160	−0.000 377
y^2	-1.36×10^{-04}	-8.66×10^{-05}	-7.58×10^{-05}	-7.38×10^{-05}	5.86×10^{-05}
z^2	0.000 458	0.000 368	0.000 266	0.000 281	0.000 384
Number of samples	125	125	125	125	125
Mean difference (%)	0.12	0.08	0.03	0.03	0.04
Max. difference (%)	6.15	5.72	3.14	4.19	7.07

are appropriate and realistic. The organ masses of the 125 used computational phantoms of the 5-year-old male are calculated and compared with the reference ICRP data at the same age in figure 2. The organ masses of the constructed phantoms and ICRP reference data are comparable and follow a similar trend across different organs/tissues. The average difference of organ masses between the developed model and the ICRP reference data is about 11%.

*3.2. AFs and S-values for F-*18

The AFs and *S*-values for F-18 were calculated for 125 computational phantoms where 46 identified organs were adopted as both source and target organs. Figure 3 shows the correlation between self-AFs of F-18 for the kidney and body weight, standing height and SSR for the 5-years-old male phantom series with statistical parameters of average values, median values, max values and min values. The Pearson correlation coefficients for the relationship between body weight, body height, BMI, SSR and sitting height and self-AF values of F-18 for representative organs are summarized in table 1. The correlation coefficients between organ self-AFs of F-18 and body weight and BMI vary within the range 0.825–0.988 and 0.608–0.968, respectively.

Figure 4 shows the calculated self-absorbed *S*-values of F-18 for the brain, liver, lung, spleen, thymus, thyroid, heart wall, kidney and adrenal of the habitus-dependent 5-years-old male phantoms with different habitus. The estimated mean self-absorbed *S*-values are in agreement with those reported by Stabin and Siegel (Stabin and Siegel 2003) and Xie *et al* (2013). The difference of self-absorbed *S*-values of F-18 between habitus-dependent phantoms and the MIRD reference phantom (Stabin and Siegel 2003) vary between −19.1% and 5.5%, while the self-absorbed *S*-values of F-18 between habitus-dependent phantoms and the predetermined phantom corresponding to the ICRP reference data vary between −16.4% and 5.2% (Xie *et al* 2013).

Figure 5 presents the correlation of self-absorbed *S*-values of F-18 for the liver with body weight, standing height and SSR for the constructed phantoms. Pearson correlation coefficients for the relationship between body habitus and self-absorbed *S*-values of F-18 for representative organs are summarized in table 2. For most organs, the self-absorbed *S*-value present strong negative correlations with body weight and BMI and weak correlations with height and SSR.

Figure 6 shows the correlation between cross-absorbed *S*-values of F-18 for the spleen irradiating the stomach with body weight, standing height and SSR. Pearson correlation coefficients for the relationship between body habitus and cross-absorbed *S*-values of F-18 for representative organ pairs are summarized in table 3. The cross-absorbed *S*-values for the total body irradiating other organs decrease with increasing body weight.

3.3. Absorbed and effective doses for ^{18}F-labelled radiotracers

The absorbed doses to 46 target organs from five ^{18}F-labelled radiotracers were calculated for the 125 considered computational phantoms. Figure 7 compares the absorbed dose of ^{18}F-FDG for representative internal organs of the constructed phantoms between the results of the ICRP 106 (ICRP 2008) for the MIRD phantom and those reported by Xie and Zaidi (2014) for the UF-NCI phantom. There is good agreement between the absorbed doses reported in these three works. The mean relative difference of the absorbed dose of ^{18}F-FDG between the constructed phantoms and the MIRD phantom for representative organs are $-1.3 \pm 19\%$. It is equal to $-8.1 \pm 5.2\%$ between the constructed phantoms and the UF-NCI phantom. Figure 8 presents the correlation between the absorbed dose of ^{18}F-FDG in the liver and body weight, standing height and SSR for the constructed 5-years-old male phantom. Pearson correlation coefficients for the relationship between body habitus and absorbed dose of ^{18}F-FDG and ^{18}F-FBPA for different organs of the used phantoms are shown in table 4.

Figure 9 shows the correlations between the effective dose of ^{18}F-FDG for the 5-years-old male phantoms and body weight, standing height and SSR. The estimated absorbed dose and effective dose commonly decreases when the total body weight increases. Table 5 summarizes the Pearson correlation coefficients for the relationship between body habitus and the effective dose of five ^{18}F-labelled radiotracers in the constructed phantoms. Pearson correlation coefficients for the relationship between different body habitus parameters indicate that the BMI presents strong statistical correlations with weight and height while sitting height presents strong statistical correlations with height, BMI and SSR (table 6). Comparisons of the effective dose of ^{18}F-Amino acids, ^{18}F-Brain receptor substances, ^{18}F-FDG, ^{18}F-L-DOPA and ^{18}F-FBPA between the constructed 5-years-old male phantoms and the predetermined phantom corresponding to the ICRP reference data (Xie *et al* 2013) are illustrated in figure 10. The coefficients of polynomial functions resulting from the fitting procedure of the effective dose of ^{18}F-Amino acids, ^{18}F-Brain receptor substances, ^{18}F-FDG, ^{18}F-L-DOPA and ^{18}F-FBPA are presented in table 7, which also lists the differences (0.04%–0.12% on average, 7.07% maximum) between the originally calculated effective dose values and the results computed using the parameterization algorithm for the same setting of body weight, height and SSR.

4. Discussion

The constructed computational phantoms represent a comprehensive anthropometric phantom series of the 5-year-old male of different habitus. For the same organ, the mean organ mass of the developed models is slightly higher than the corresponding ICRP reference organ mass because the US peadiatric population as reported in the NHANES study has a higher average body weight and BMI compared to the ICRP reference children of the same age.

F-18 is the most widely used positron-emitting radionuclide used in preclinical research and clinical setting. It can be employed as a substitute for hydrogen or fluorine in the molecule of interest to produce molecular imaging probes for PET imaging. In this work, we calculated AFs of F-18 and the absorbed and effective doses of five ^{18}F-labelled radiotracers in 125

5-year-old computational male phantoms covering statistical distributions of body morphometry of the 5-year-old North-American child. In these 125 computational phantoms, the self-AFs of F-18 of most organs increase with total body weight and BMI. In contrast, the self-absorbed *S*-values of F-18, and absorbed and effective doses of ^{18}F-labelled radiotracers decrease with body weight and BMI. Most investigated dosimetric quantities present weak correlations with height and SSR, except the cross-absorbed *S*-values (table 3 and figure 6). Among all the considered morphometric parameters, total body weight and BMI show the strongest statistical correlations with most internal radiation dosimetry results.

The dosimetric characteristics of positron-emitting radionuclides and radiotracers were compared between the constructed phantoms of various habitus, the MIRD stylized phantom and the standard computational phantom corresponding to the ICRP reference anatomic data. For self-absorbed *S*-values of F-18 in the liver, the relative differences between the habitus-dependent phantoms and the MIRD stylized phantom is $4.6 \pm 14.7\%$ while the differences between the habitus-dependent phantoms and the UF-NCI phantom is $2.2 \pm 14.3\%$. For absorbed doses of ^{18}F-FDG in the kidney, the relative differences between habitus-dependent phantoms and the ICRP 106 recommendations is $-22.4 \pm 9.2\%$ while the differences between habitus-dependent phantoms and the UF-NCI phantom is $-12.7 \pm 10.3\%$. In terms of effective doses, the mean absolute differences between the constructed phantoms of different habitus and the fixed UF-NCI model for ^{18}F-Amino acids, ^{18}F-Brain receptor substances, ^{18}F-FDG, ^{18}F-L-DOPA and ^{18}F-FBPA are 11.4%, 11.3%, 10.8%, 13.3% and 11.4%, respectively. For patients at the same age, radiation dose estimates based on predetermined reference models provide accurate dose estimation for population having similar habitus as the ICRP reference data. However, a deviation of about 10% may be observed between the predetermined reference model and individual subjects presenting with different habitus. Table 7 revealed that the coefficient of the *x*-term is much larger than that of the *y*- and *z*-terms, which indicates the stronger dependence of the effective dose on body weight than on body height and SSR.

5. Conclusion

Based on a hybrid computational phantom, patient-specific phantom can be created to reflect their body morphometries, thus offering the opportunity to perform patient-specific dosimetry calculations under different radiation exposure conditions. A comprehensive evaluation of the internal dosimetry charateristics of F-18 and ^{18}F-labelled radiotracers was performed using the constructed library of 5-year-old computational phantoms with different habitus. The impact of total body weight, standing height, sitting height, BMI and SSR on the calculation of AFs and *S*-values of F-18 and absorbed dose and effective dose of ^{18}F-labelled radiotracers was investigated. Most dosimetric parameters present strong negative statistical correlations with total body weight and BMI but weak correlations with the height and SSR, confirming that phantoms representing slimmer individuals may receive higher organ absorbed doses. The obtained correlations between body morphometric parameters and dosimetric quantities in the 5-year-old group are expected to be similar in subjects of other sex and of other ages. The dosimetric analysis for the 5-year-old computational phantom was used as an example demonstrating the usefulness of the developed computational phantom library (Xie *et al* 2017) where the impact of body habitus on internal radiation dosimetry calculations is highlighted. An extension to other computational models of various sex/ages is straightforward and will be conducted in future studies. The dose comparisons between habitus-dependent phantoms and predefined phantoms corresponding to ICRP reference data provided a quantitative evaluation of the uncertainties involved in the utilization of predefined reference phantoms to estimate

the internal dose for individual patients. It was concluded that patient radiation dose estimates based on the most closely matched habitus-dependent phantom should be considered. The detailed analysis of habitus-dependent dosimetric results for the 5-year-old child further supports the arguments for individual patient dose assessment.

Acknowledgments

This work was supported by the Swiss National Science Foundation under grant SNSF 31003A-149957.

Conflict of interest statement

The authors declare that they have no conflict of interest.

References

Bolch W E, Eckerman K F, Sgouros G and Thomas S R 2009 MIRD Pamphlet No. 21: a generalized schema for radiopharmaceutical dosimetry—standardization of nomenclature *J. Nucl. Med.* **50** 477–84

Christ A *et al* 2010 The virtual family-development of surface-based anatomical models of two adults and two children for dosimetric simulations *Phys. Med. Biol.* **55** N23–38

de la Grandmaison G L, Clairand I and Durigon M 2001 Organ weight in 684 adult autopsies: new tables for a Caucasoid population *Forensic Sci. Int.* **119** 149–54

Fahey F H, Ziniel S I, Manion D, Baker A and Treves S T 2016 Administered activities in pediatric nuclear medicine and the impact of the 2010 North American consensus guidelines on general hospitals in the United States *J. Nucl. Med.* **57** 1478–85

Frisancho A R 2008 *Anthropometric Standards: an Interactive Nutritional Reference of Body Size and Body Composition for Children and Adults* (Ann Arbor, MI: University of Michigan Press)

Gosselin M-C, Neufeld E, Moser H, Huber E, Farcito S, Gerber L, Jedensjö M, Hilber I, Di Gennaro F and Lloyd B 2014 Development of a new generation of high-resolution anatomical models for medical device evaluation: the Virtual Population 3.0 *Phys. Med. Biol.* **59** 5287–303

HPS 2012 Radionuclide decay data http://hps.org/publicinformation/radardecaydata.cfm

Huang B, Law M W and Khong P L 2009 Whole-body PET/CT scanning: estimation of radiation dose and cancer risk *Radiology* **251** 166–74

Huang C and McConathy J 2013 Radiolabeled amino acids for oncologic imaging *J. Nucl. Med.* **54** 1–4

ICRP 1987 ICRP Publication 53: radiation dose to patients from radiopharmaceuticals *Ann. ICRP* **18** 1–76

ICRP 1998 ICRP Publication 80: radiation dose to patients from radiopharmaceuticals—addendum to ICRP Publication 53 *Ann ICRP* **28** 1–126

ICRP 2002 ICRP Publication 89: basic anatomical and physiological data for use in radiological protection: reference values *Ann. ICRP* **32** 5–265

ICRP 2007 ICRP Publication 103: the 2007 recommendations of the international commission on radiological protection *Ann. ICRP* **37** 1–332

ICRP 2008 ICRP Publication 106: radiation dose to patients from radiopharmaceuticals—addendum 3 to ICRP Publication 53 *Ann. ICRP* **38** 1–197

Lee C, Lee C, Williams J L and Bolch W E 2006 Whole-body voxel phantoms of paediatric patients—UF series B *Phys. Med. Biol.* **51** 4649–61

Lee C, Lodwick D, Hasenauer D, Williams J L and Bolch W E 2007 Hybrid computational phantoms of the male and female newborn patient: NURBS-based whole-body models *Phys. Med. Biol.* **52** 3309–33

Lee C, Williams J L, Lee C and Bolch W E 2005 The UF series of tomographic computational phantoms of pediatric patients *Med. Phys.* **32** 3537–48

Li X, Zhang D and Liu B 2013 A parameterization method and application in breast tomosynthesis dosimetry *Med. Phys.* **40** 092105

Lloyd B, Cherubini E, Farcito S, Neufeld E, Baumgartner C and Kuster N 2016 Covering population variability: morphing of computation anatomical models. *Simulation and Synthesis in Medical Imaging: 1st Int. Workshop, SASHIMI 2016, Held in Conjunction with MICCAI 2016 Proc. (Athens, Greece, 21 October 2016)* ed S A Tsaftaris *et al* (Cham: Springer) pp 13–22

McDowell M A, Fryar C D, Ogden C L and Flegal K M 2008 Anthropometric reference data for children and adults: United States, 2003–2006 *Natl Health Stat. Rep.* **10** 1–44 (www.cdc.gov/nchs/data/nhsr/nhsr010.pdf)

Molina D K and DiMaio V J 2015 Normal organ weights in women: part II—the brain, lungs, liver, spleen, and kidneys *Am. J. Forensic Med. Pathol.* **36** 182–7

Oehme L, Perick M, Beuthien-Baumann B, Wolz M, Storch A, Löhle M, Herting B, Langner J, van den Hoff J and Reichmann H 2011 Comparison of dopamine turnover, dopamine influx constant and activity ratio of striatum and occipital brain with ^{18}F-dopa brain PET in normal controls and patients with Parkinson's disease *Eur. J. Nucl. Med. Mol. Imaging* **38** 1550–9

Pelowitz D 2005 *MCNPX Version 2.5. 0 User's Manual* (Los Alamos, NM: Los Alamos National Laboratory) LA-CP-05-0369

Reivich M, Alavi A and Wolf A 1985 Glucose metabolic rate kinetic model parameter determination in humans: the lumped constant and rate constants for [^{18}F]fluorodeoxyglucose and [^{11}C] deoxyglucose *J. Cereb. Blood Flow Metabol.* **5** 179–92

Robbins E 2008 Radiation risks from imaging studies in children with cancer *Pediatr. Blood Cancer* **51** 453–7

Sheikhazadi A, Sadr S S, Ghadyani M H, Taheri S K, Manouchehri A A, Nazparvar B, Mehrpour O and Ghorbani M 2010 Study of the normal internal organ weights in Tehran's population *J. Forensic Leg. Med.* **17** 78–83

Stabin M G 1996 MIRDOSE: personal computer software for internal dose assessment in nuclear medicine *J. Nucl. Med.* **37** 538–46 (PMID: 8772664)

Stabin M G and Siegel J A 2003 Physical models and dose factors for use in internal dose assessment *Health Phys.* **85** 294–310

Stabin M G, Sparks R B and Crowe E 2005 OLINDA/EXM: the second-generation personal computer software for internal dose assessment in nuclear medicine *J. Nucl. Med.* **46** 1023–7 (PMID: 15937315)

Steinert M, Weiss M, Gottlöber P, Belyi D, Gergel O, Bebeshko V, Nadejina N, Galstian I, Wagemaker G and Fliedner T M 2003 Delayed effects of accidental cutaneous radiation exposure: fifteen years of follow-up after the Chernobyl accident *J. Am. Acad. Dermatol.* **49** 417–23

Xie T, Bolch W E, Lee C and Zaidi H 2013 Pediatric radiation dosimetry for positron-emitting radionuclides using anthropomorphic phantoms *Med. Phys.* **40** 102502–14

Xie T, Kuster N and Zaidi H 2017 Computational hybrid anthropometric paediatric phantom library for internal radiation dosimetry *Phys. Med. Biol.* **62** 3263–83

Xie T and Zaidi H 2014 Evaluation of radiation dose to anthropomorphic paediatric models from positron-emitting labelled tracers *Phys. Med. Biol.* **59** 1165–87

Xu X G 2014 An exponential growth of computational phantom research in radiation protection, imaging, and radiotherapy: a review of the fifty-year history *Phys. Med. Biol.* **59** R233–302

Xu X G and Eckerman K F (ed) 2009 *Handbook of Anatomical Models for Radiation Dosimetry* (Boca Raton, FL: CRC Press)

Yoshimoto M, Kurihara H, Honda N, Kawai K, Ohe K, Fujii H, Itami J and Arai Y 2013 Predominant contribution of L-type amino acid transporter to 4-borono-2-18F-fluoro-phenylalanine uptake in human glioblastoma cells *Nucl. Med. Biol.* **40** 625–9

Zaidi H 1999 Relevance of accurate Monte Carlo modeling in nuclear medical imaging *Med. Phys.* **26** 574–608

Zaidi H and Xu G 2007 Computational anthropomorphic models of the human anatomy: the path to realistic Monte Carlo modeling in radiological sciences *Annu. Rev. Biomed. Eng.* **9** 471–500